Chemical Engineering Science 77 (2012) 235–241

Contents lists available at SciVerse ScienceDirect

Chemical Engineering Science

journal homepage: www.elsevier.com/locate/ces

Identification of nucleation rates in droplet-based microfluidic systems

K. Chen [a], L. Goh [a], G. He [b], P.J.A. Kenis [a], C.F. Zukoski III [a], R.D. Braatz [a,b,*]

[a] Department of Chemical & Biomolecular Engineering, University of Illinois at Urbana-Champaign, 600 South Matthews Avenue, Urbana, IL 61801, USA
[b] Department of Chemical Engineering, Massachusetts Institute of Technology, 77 Massachusetts Avenue, Cambridge, MA 02139, USA

ARTICLE INFO

Article history:
Received 10 September 2011
Received in revised form
18 March 2012
Accepted 20 March 2012
Available online 29 March 2012

Keywords:
Crystallization
Kinetics
Nucleation
Parameter identification
Particle formation
Pharmaceuticals

ABSTRACT

Characterization of the rate of nucleation of crystals from solution continues to be of interest, both for investigations into fundamental molecular phenomena as well as for applications in the pharmaceuticals, biotechnology, and fine chemicals industries. Substantial experimental evidence indicates that nucleation in some solute-solvent systems does not agree with classical theory, especially at high supersaturations. An approach is proposed for computing bounds on the nucleation rate as a function of supersaturation that does not require an assumed analytical expression for the nucleation kinetics. The approach involves (1) a microfluidic platform that measures crystal nuclei formation in droplets, (2) the analytical solution of the Chemical Master equation for nucleation that takes finite-volume effects into account, and (3) a numerical algorithm that employs linear splines to construct upper and lower bounds on the nucleation rate from the experimental data produced by the microfluidic platform. The approach is demonstrated for mean induction times measured for the nucleation of paracetamol and glycine crystals in aqueous solution. The approach can be used to suggest dependencies for the development of new nucleation expressions and for providing kinetic information needed for the simulation of crystallizers that operate at high supersaturations, such as dual-impinging-jet and vortex-mixer crystallizers.

1. Introduction

Numerous studies have been directed towards obtaining a better fundamental understanding of nucleation mechanisms (Blow et al., 1994; ten Wolde and Frenkel, 1997; Saikumar et al., 1998; Aizenberg et al., 1999; Baird, 1999; Cacciuto et al., 2004; Schope et al., 2006; Li et al., 2008; Kreutz et al., 2009; Auer and Frenkel, 2001). Substantial experimental evidence has been published (Vekilov, 2004; 2010) that shows that nucleation rate expressions for some solute-solvent systems do not agree with classical nucleation theory (Volmer and Weber, 1926; Nielsen, 1964; Nyvlt, 1985) at the high supersaturations that can occur during protein crystallization, dual-impinging-jet and vortex-mixer crystallization of pharmaceuticals, and microfluidic crystallizations of various compounds (Midler et al., 1994; Dauer et al., 1996; Mahajan and Kirwan, 1996; Sanjoh and Tsukihara, 1999; Lindrud et al., 2001; am Ende et al., 2003; Zheng et al., 2003; Schwarzer and Peukert, 2004; Vekilov, 2004; 2010; Squires and Quake, 2005; Hansen et al., 2006; Wang et al., 2006; Liu et al., 2008). For example, the nucleation rate has been experimentally observed to go through a maximum and then decrease with respect to supersaturation for some systems (e.g., see Kelton, 1991; Pusey, 1991). As another example, the experimentally determined homogeneous nucleation rate for lysozyme crystals in 4% NaCl-aqueous solution has been reported (Vekilov, 2004) with (1) a plateau in the nucleation rate with respect to lysozyme concentration, and (2) a bifurcation of the nucleation rate into two branches corresponding to the formation of two crystal morphologies at the same lysozyme concentration.

No quantitative replacement for classical nucleation theory has been established yet, which presents a quandary for engineers who need rate expressions to characterize nucleation kinetics at high supersaturation for incorporation into mathematical models for the design of crystallizers that employ process intensification (e.g., Schwarzer and Peukert, 2004; Liu et al., 2008; Woo et al., 2009). A crystallizer could produce poor quality product if designed based on a rate expression that is not valid for the particular solute(s), solvent(s), and supersaturation range of interest. This paper addresses this problem by proposing an approach for determining upper and lower bounds on the nucleation rate as a function of supersaturation that does not require any assumptions on the specific form for the nucleation rate expression. These bounds also could be used to design subsequent experiments that will generate data that maximally

* Corresponding author at: University of Illinois at Urbana-Champaign, Department of Chemical & Biomolecular Engineering, Massachusetts Institute of Technology, 77 Massachusetts Avenue, Cambridge, MA 02139, United States. Tel.: +1 617 253 3112; fax: +1 617 258 0546.
E-mail address: braatz@mit.edu (R.D. Braatz).

0009-2509/$ - see front matter © 2012 Elsevier Ltd. All rights reserved.
http://dx.doi.org/10.1016/j.ces.2012.03.026

reduce the gap between the upper and lower bounds on the nucleation rate.

The approach consists of three components. The first component is a microfluidic platform that measures crystal nuclei formation in droplets (e.g., Sanjoh and Tsukihara, 1999; Zheng et al., 2003; Vekilov, 2004; 2010; Squires and Quake, 2005; Hansen et al., 2006; Li et al., 2008; Kreutz et al., 2009; Talreja et al., 2005). The nucleation data can be reported in any form, such as mean induction times, induction time distributions, or the number of crystals generated in multiple droplets over time. The second component is the Chemical Master equation for nucleation that satisfies mass conservation while taking finite-volume effects into account (Goh, 2007; Goh et al., 2010). The third component of the approach is a numerical algorithm that employs linear splines to construct upper and lower bounds on the nucleation rate from the experimental data produced by the microfluidic platform and an analytical solution for the Chemical Master equation. After describing the second and third components of this approach in more detail, the approach is demonstrated for the nucleation of paracetamol and glycine crystals in an evaporation-based microfluidic platform.

2. Theoretical methods

2.1. Analytical solution to the chemical master equation

The Chemical Master equation for nucleation that satisfies mass conservation while taking finite-volume effects into account is Goh et al. (2010):

$$\frac{dP_0(t)}{dt} = -\kappa(t)P_0(t), \quad P_0(0) = 1, \tag{1a}$$

$$\frac{dP_n(t)}{dt} = \kappa(t)(P_{n-1}(t) - P_n(t)), \quad P_n(0) = 0, \quad n = 1,2,\ldots \tag{1b}$$

where $P_n(t)$ is the probability that a droplet contains n crystals and $\kappa(t)\,dt$ is the probability that a critical nucleus will form during an infinitesimal time interval dt. The model assumes that the time to grow from a nucleus to a visible crystal is negligible compared to the induction time, which is a very good assumption for nucleation in micro- to nanoliter drops at high supersaturation for most systems (e.g., see analysis in Goh et al. (2010) and references cited therein).[1] The differential equations (1) describe a non-stationary Poisson process (Cinlar, 1971) and can be solved analytically to obtain the time evolution of the above probabilities.[2]

The average number of crystals that form over time for a large number of droplets, the induction time distribution, the variance in the induction times, and the mean, most likely, and median induction times can be derived from this analytical solution. For example, the mean induction time t_{mean} for the nucleation of at least 1 crystal in a droplet is

$$t_{mean} = \int_0^\infty t\kappa(t) e^{-\int_{t_{sat}}^{t} \kappa(s)ds} dt \tag{2}$$

where t_{sat} is the time when the solute concentration in the drop just reaches the saturated solute concentration. The analytical expressions for all of the measurable quantities such as in Eq. (2) can be computed for any expression for $\kappa(t) \geq 0$ by using standard subroutines for numerical integration (e.g., Chapra and Canale, 2002; Heath, 2002). For homogeneous nucleation or heterogeneous nucleation on tiny particles distributed with a well-mixed droplet, the supersaturation-dependent nucleation rate $J(S(t))$ is related to $\kappa(t)$ in (1) by $\kappa(t) = J(S(t))V(t)$ where V is the droplet volume. The time trajectory for the supersaturation $S(t)$ and volume $V(t)$ can be directly measured or derived from mass balances on the solute(s), solvent(s), and precipitant(s) in a droplet, so that $\kappa(t) = J(S(t))V(t)$ can be computed for any specified expression for the nucleation rate $J(S)$. For heterogeneous nucleation on any contact surface or interface of area $A(t)$, the corresponding relationship is $\kappa(t) = J(S(t))A(t)$.

2.2. Construction of bounds on the nucleation rate

A numerical algorithm employing a model-free representation is used to construct upper and lower bounds on the nucleation rate $J(S)$ from the experimental data produced by the microfluidic platform and the analytical solutions for the model Eq. 1. The nucleation rate is parameterized by the piecewise-linear function (also called a first-order spline or a *linear spline*):

$$J(S) = a_i S + b_i \quad \text{for} \quad S_{i-1} < S < S_i, \; i = 1,2,\ldots,n, \tag{3}$$

where S_i are discrete values for the supersaturation, and $b_i = b_{i-1} + (a_{i-1} - a_i)S_{i-1}$ ensures continuity and $b_1 = 0$ so that $J = 0$ for $S = 0$. The coefficients were selected so that $J(S) \geq 0$ for $S \geq 0$ and to be finite, which bounds the derivative with respect to the supersaturation. The non-equal spacing allows higher resolution for small values for S. This parameterization allows the nucleation rate $J(S)$ to be increasing, decreasing, or at a plateau for any range of supersaturation, which is flexible enough to describe the deviations from classical nucleation theory that have been reported in the literature (e.g., see Vekilov, 2004; 2010; and citations therein).

The numerical algorithm determines the set of constrained coefficients in the linear spline that are consistent with an upper bound on the sum-of-squared deviations (SSD) between the model and measurements,

$$SSD(\theta) = \sum_{i=1}^{N} [y_{model,i} - y_{measured,i}(\theta)]^2 \leq \varepsilon, \tag{4}$$

where N is the number of experimental data points, $y_{measured,i}$ is the ith data point, and $y_{model,i}$ is the corresponding value computed from the Chemical Master equation (1) with the linear spline for $J(S)$, θ is the vector of coefficients a_i and b_i, and the value of the upper bound ε is computed from the intrinsic variability in the measured values as well as imperfections in the experiments that result in variations in the evaporation rate, initial solute concentration, and droplet volume (for details, see Goh, 2007). The value for ε can be a function of a confidence level α if estimated by statistical procedures (Beck and Arnold, 1977; Taylor, 1982). For the case in which each data point is the measured mean induction time t_{ind} for repeated experiments, Eq. (4) would be

$$SSD(\theta) = \sum_{i=1}^{N} \left[t_{ind,model,i} - t_{ind,measured,i}(\theta)\right]^2 \leq \varepsilon \tag{5}$$

In this approach, a bound on the smoothness of the nucleation rate can be included, which is written as $\sum_i (a_{i+1} - a_i)^2 \leq \gamma$. In any case, sets of coefficients a_i and b_i that satisfy these bounds can be located by stochastic search (Foster et al., 1993). A best-fit nucleation rate can be obtained by minimization of the left-hand side of Eq. (4) subject to the smoothness constraint or by

[1] If the time required to grow a crystal to a detectable size is not negligible, then subtract this time from the measured induction times before applying the expressions in this paper.

[2] The analytical solution to Eq. (1) is $P_n(t) = (1/n!)[\int_0^t \kappa(s)ds]^n e^{-\int_0^t \kappa(s)ds}$, $n = 0,1,2,\ldots$ (Goh et al., 2010).

incorporating smoothness through a penalty term:

$$\min_{\theta}\left\{\sum_{i=1}^{N}[y_{\text{model},i}-y_{\text{measured},i}(\theta)]^2+\hat{\gamma}\sum_{i}(a_{i+1}-a_i)^2\right\} \quad (6)$$

By replacing the functional form for $J(S)$, the above approach can be used to evaluate the consistency of experimental data with a particular nucleation expression, such as that for classical nucleation theory (Nielsen, 1964; Walton, 1969),

$$J(S(t))=AC(t)\exp(-B/(\ln(S(t)+1)))^2) \quad (7)$$

where $C(t)$ is the solute concentration and A and B are model parameters. The low number of parameters within power-law, classical nucleation, and other simple expressions enables the family of $J(S)$ consistent with those expressions to be determined by gridding the parameters. Upper and lower bounds on the nucleation rate $J(S)$ can also be computed from the maximum and minimum value of each linear spline at each value of the supersaturation. A plotting algorithm can order the linear splines into groups that simplify the interpretation of nucleation rates that are consistent with the experimental data. The lack of linear splines that are monotonically increasing would indicate that the nucleation expression is not a monotonically increasing function of the supersaturation. In the case of multiple distinct values for the nucleation rate $J(S)$, as would occur for the branch reported for lysozyme (Vekilov, 2004), two bands of allowed nucleation rates would be computed if values between the bands are inconsistent with the experimental data.

The proposed approach is demonstrated for two examples below.

3. Results and discussion

Consider the measurement of mean induction times for paracetamol and glycine in aqueous solution for an array of conditions in an evaporation-based microwell platform of hanging droplets (for details on the experimental system, see Talreja et al., 2007).[3] No crystals were observed on the droplet support so nucleation was assumed to occur in the liquid phase, in which case the mean induction time is given by inserting the product of the nucleation rate per unit volume, J, and the volume V into Eq. (2) to give

$$t_{\text{ind}}=\int_0^{\infty} tJ(S(t))V(t)e^{-\int_{t_{\text{sat}}}^{t}J(S(s))V(s)\mathrm{d}s}\mathrm{d}t, \quad (8)$$

where S in this study was taken to be the relative supersaturation (the same approach also applies to absolute supersaturation) and $V(t)=V_0(1-\beta t)$ was computed from a mass balance on the solvent (Talreja et al., 2007), where β is the mass evaporation rate (ER) divided by the initial mass of solvent.

3.1. Nucleation of paracetamol

Measured mean induction times for paracetamol in aqueous solution for different initial solute concentrations (C_0) and evaporation rates (ER) and the solute concentrations at the time that crystals were first observed (referred to as *metastable concentrations*) are shown in Fig. 1. The mean induction times decrease with increased evaporation rate (Fig. 1), as expected. Many linear splines are consistent with the data within the experimental variations (see Fig. 2), with the splines showing a monotonic dependence on the supersaturation such as occurs for classical nucleation theory (Fig. 2(b)). The experimentally measured mean induction times

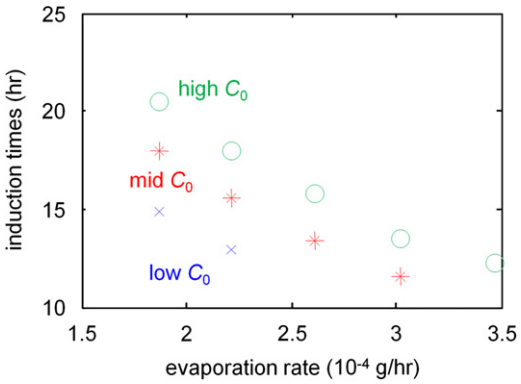

Fig. 1. Mean induction times, mass evaporation rates (ER), and initial concentrations (C_0) for 11 sets of experimental conditions for the nucleation of paracetamol in aqueous solution at 21 °C (C_{sat} = 13.2 g paracetamol/kg water). The initial volume was 5.07 μL and the low, mid, and high initial solute concentrations C_0 are given in Table 1.

Table 1
Experimental data for measuring mean induction times for paracetamol in aqueous solution (Goh et al., 2010). The initial droplet volume was 5.07 μL for all experiments.

Experiment No.	Mass evaporation rate (g/h)	Initial solution concentration (g solute/kg solvent)	Mean time to reach saturated conditions and observe at least one crystal (h)	Measured true induction time (h)*
1	2.22E−04	7.94	22.00	12.9
2	1.87E−04	7.94	25.67	14.9
3	3.02E−04	9.90	15.75	11.6
4	2.61E−04	9.90	18.25	13.4
5	2.22E−04	9.90	21.25	15.5
6	1.87E−04	9.90	24.75	18.0
7	3.47E−04	11.86	13.75	12.3
8	3.02E−04	11.86	15.25	13.5
9	2.61E−04	11.86	17.75	15.8
10	2.22E−04	11.86	20.25	17.9
11	1.87E−04	11.86	23.25	20.5

* The last column was determined by subtracting the time required for the droplet to reach saturated conditions from the second to last column.

were consistent with a classical nucleation model (Fig. 3). The minimum sum-of-squared deviations for the linear spline is very close to that for the classical nucleation expression, which implies that the mean induction time data for paracetamol in aqueous solution in Fig. 1 provide no evidence that the nucleation rate deviates significantly from that predicted by classical nucleation theory.

3.2. Nucleation of glycine

Mean induction times measured for glycine in aqueous solution for different initial solute concentrations (C_0) and evaporation rates (ER) and metastable concentrations are shown in Fig. 4. The mean induction times decrease with increased evaporation rate for low to mid initial solute concentrations with this dependence being much weaker for high initial solute concentrations (Fig. 4). The mean induction times for glycine increase with decreased initial solute concentration, which is the opposite trend observed for paracetamol (compare Figs. 1 and 4). None of the linear splines for the nucleation rate $J(S)$ produce estimates of the mean induction times that are consistent with the experimental variations (see Fig. 5(a)). Also, the linear splines that provided the best fit or nearly the best fit to the mean induction time data showed a non-monotonic dependence on the supersaturation, which is not consistent with a single classical

[3] The *induction time* is the time in which at least one crystal is observed in a droplet using an optical microscope positioned over the droplet. The measured *mean induction time* was the average of the induction times measured for three droplets that undergo the same experimental conditions, that is, have the same temperature, evaporation rate, initial concentrations, and droplet volume.

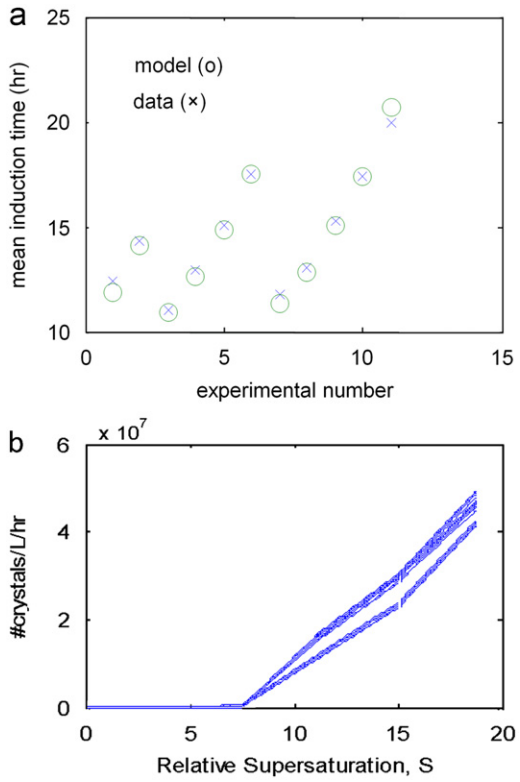

Fig. 2. (a) Mean induction times for the linear spline $J(S)$ that best fits the data reported in Fig. 1 (paracetamol), with $SSD = 1.4 < \varepsilon = 3.8$, (b) sample nucleation rates parameterized by linear splines that are consistent with experimental variations of $\varepsilon = 3.8$.

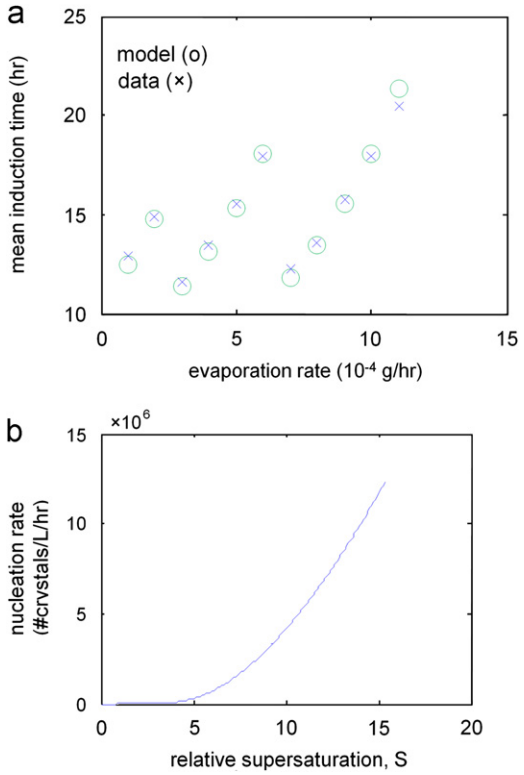

Fig. 3. (a) Mean induction times for the classical nucleation expression $J(S)$ that best fits the data reported in Fig. 1 (paracetamol), with $A = 3.9 \times 10^5$, $B = 15.0$, and $SSD = 1.46 < \varepsilon$, (b) the corresponding nucleation rate.

Table 2
Experimental data for measuring mean induction times for glycine in aqueous solution.

Experiment No.	Mass evaporation rate (g/h)	Initial solution concentration (g solute/kg solvent)	Initial droplet volume (μL)	Mean time to reach saturated conditions and observe at least one crystal (h)	Measured true induction time (h)*
1	4.46E−04	173.55	4.50	9.33	6.1
2	3.68E−04	173.55	4.50	10.11	6.2
3	2.98E−04	173.55	4.50	11.50	6.6
4	2.36E−04	173.55	4.50	13.00	6.9
5	1.79E−04	173.55	4.50	15.67	7.6
6	4.46E−04	200.00	4.35	5.33	3.2
7	3.68E−04	200.00	4.35	5.83	3.2
8	2.98E−04	200.00	4.35	6.92	3.7
9	2.36E−04	200.00	4.35	7.89	3.9
10	1.79E−04	200.00	4.35	9.83	4.5
11	4.46E−04	209.49	4.30	4.67	2.9
12	3.68E−04	209.49	4.30	5.08	3.0
13	2.98E−04	209.49	4.30	5.67	3.0
14	2.36E−04	209.49	4.30	6.33	3.0
15	1.79E−04	209.49	4.30	7.33	3.0

* The last column was determined by subtracting the time required for the droplet to reach saturated conditions from the second to last column.

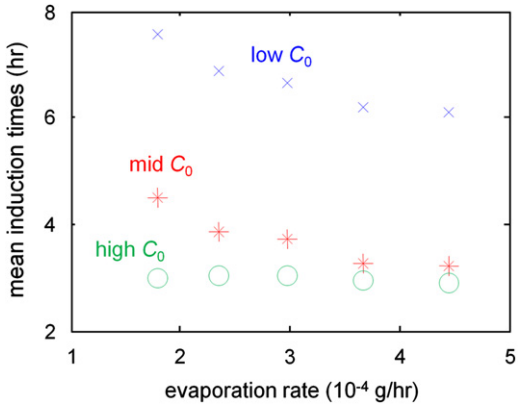

Fig. 4. Mean induction times, evaporation rates (ER), and initial concentrations (C_0) for 15 sets of experimental conditions for the nucleation of glycine in aqueous solution at 36 °C ($C_{sat} = 256.2$ g glycine/kg water). The initial droplet volumes, evaporation rates, and low, mid, and high values of the initial solute concentrations C_0 are given in Table 2.

nucleation mechanism occurring within uniform well-mixed droplets (Fig. 5(b)). In particular, the nucleation rates most consistent with the experimentally observed mean induction times have a peak located between relative supersaturation of 5 and 6, followed by another rise in nucleation rate for large supersaturation ($S > 6$, see Fig. 5(b)).

Non-monotonic dependency of the nucleation rate on supersaturation has been reported for many systems (Kelton, 1991; Pusey, 1991), with reduction in the nucleation rate with increased supersaturation attributed to a lower rate of growth of nuclei or to an increase of the solid-liquid interfacial free energy with increased supersaturation (e.g., Auer and Frenkel, 2001), but these hypotheses would not explain an increase in nucleation rate at even higher supersaturations (Fig. 5(b)). A partial explanation for the reduction of the nucleation rate for intermediate supersaturation could be the existence of multiple parallel nucleation pathways (Vekilov, 2004), in which one nucleation pathway becomes

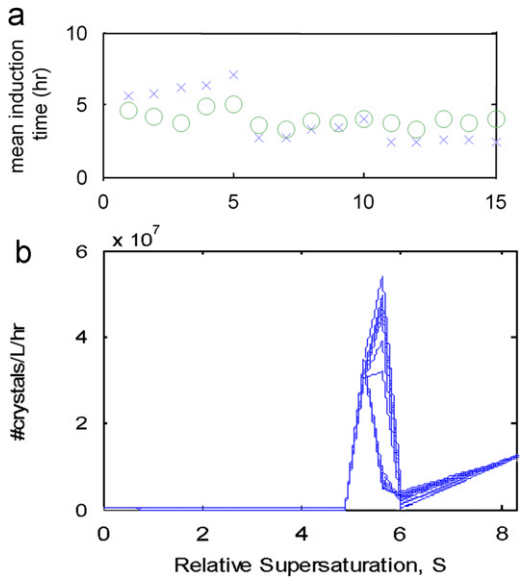

Fig. 5. (a) Mean induction times for the linear spline $J(S)$ with $n=32$ and smoothing factor $\gamma=2\times10^{-18}$ that best fits the data reported in Fig. 4 (glycine), with $SSD=37.3>\varepsilon=28.3$, with the horizontal axis being the experiment number, (b) nucleation rates parameterized by linear splines with $SSD<40$. Since there were more experiments with a metastable supersaturation S_{met} less than 3, the linear spline was chosen to have a smaller spacing between points for low S.

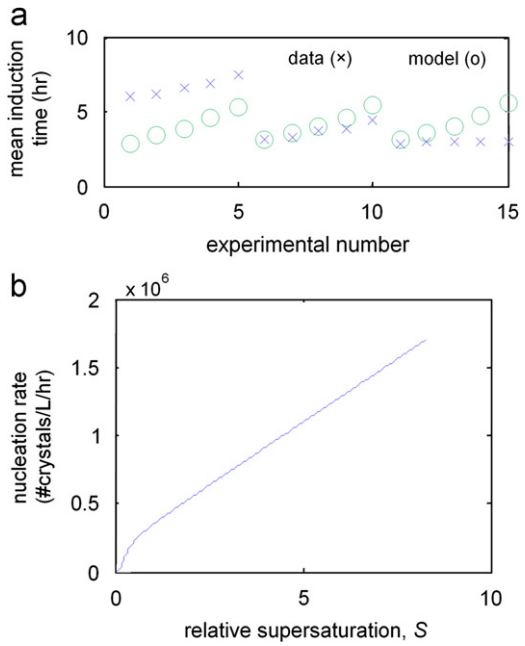

Fig. 6. (a) Best-fit mean induction times to the classical nucleation expression for the data reported in Fig. 4 (glycine), with $A=721$, $B=0.04$, and $SSD=48.7>\varepsilon$, with the horizontal axis being the experiment number, (b) the best-fit nucleation rate parameterized by the best-fit classical nucleation expression, which is inconsistent with experimental variations of $\varepsilon=28.3$.

suppressed at some supersaturation whereas a second pathway is only important at a much higher supersaturation. Different polymorphs have different nucleation pathways and typically different nucleation rates (see Allen et al., 2002 and Chen et al., 2011 for discussions of polymorphic crystal nucleation in droplets), however, only a single polymorphic form of glycine (δ) has been observed in over 100 experiments in this microfluidic platform at these evaporation rates (He et al., 2006). A possible explanation would be heterogeneous nucleation on contaminating particles in each droplet at lower supersaturation becoming covered by crystals, and so are no longer available for inducing nucleation, followed by homogeneous nucleation at higher supersaturation (Vekilov and Galkin, 2003). Another possible explanation for multiple peaks would be the presence of contaminating particles only in some of the droplets (Pound and Lamer, 1952; Laval et al., 2008; Teychené and Biscans, 2011), so that the lower supersaturation peak corresponds to droplets with the particles and the higher supersaturation increase corresponds to droplets without the particles. Of the above potential explanations for the supersaturation dependence in Fig. 5(b), the latter could explain why the best-fit linear spline did not reduce the sum-of-squared deviations below the experimental variations (see Fig. 5(a)). Another possible explanation could be that the nucleation for glycine in aqueous solution follows a two-step nucleation mechanism at high supersaturation, in which crystal nucleation occurs after a liquid-liquid phase separation that forms highly concentrated droplets within each droplet (Vekilov, 2010). Some experimental evidence from small-angle x-ray scattering for such a two-step nucleation mechanism in glycine in aqueous solution has been reported (Chattopadhyay et al., 2005).

As expected from the lack of monotonicity of the nucleation rate in Fig. 5(b), the experimentally measured mean induction times were not consistent with the best-fit classical nucleation model (Fig. 6), which produced much larger sum-of-squared deviations than for the best-fit linear spline (Fig. 5). The analysis in Figs. 5 and 6 provide evidence that nucleation within the droplets for this set of experiments was not described by a single classical nucleation mechanism occurring within uniform well-mixed droplets.

Most of the aforementioned possible explanations for observing an apparent deviation from classical nucleation theory involve multiple nucleation pathways. An approach for applying the method to address systems with multiple nucleation pathways is to separate the data into groups and independently estimate the bounds on the nucleation rates for each group of data. For example, the above hypothesis of two nucleation mechanisms occurring over the supersaturation range can be further evaluated by repeating the analysis with the mean induction time data for the highest supersaturations removed from the data set (see Fig. 7(a)). Many linear splines were consistent with this subset of the data, and these linear splines showed no evidence of a nonmonotonic dependence of the nucleation rate on the supersaturation (Fig. 7(b)). This analysis supports the hypothesis that evidence for a deviation from the classical nucleation mechanism only occurs for the mean induction time data at high supersaturations. The nucleation rate for the best-fit classical nucleation expression is within experimental variations, indicating that the mean induction time data for relative supersaturations less than 0.73 are reasonably consistent with classical nucleation theory (Fig. 8). A non-classical nucleation theory is indicated only for the mean induction time data in which the relative supersaturation within the droplets is higher than 0.73.

The above approach of separating the data in multiple sets that are subsequently analyzed independently can be applied when it is clear how the droplets should be separated into multiple data sets, such as in the above example where the droplets were separated into terms of low and high supersaturation. When each droplet cannot be *a priori* assigned to a different nucleation pathway, then the model (1) can still be written for the droplets associated with each nucleation pathway, but an additional assumption is needed to be able to combine the model predictions from multiple nucleation pathways to compute experimental observations such as mean induction times. For example, if the droplets had varying numbers of contaminants, then an assumption could be that the source solution has a spatially uniform

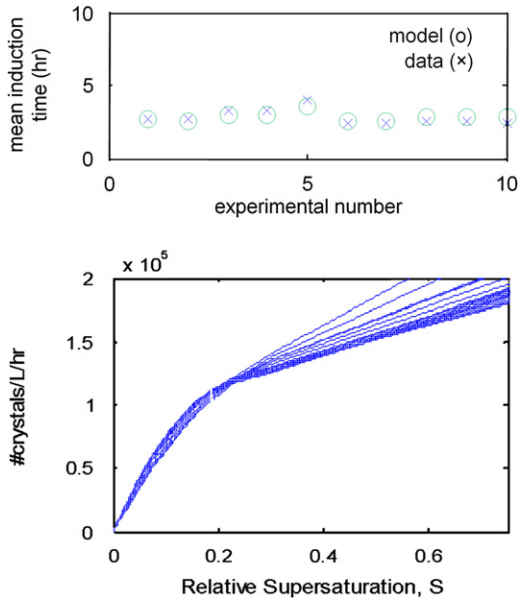

Fig. 7. (a) Mean induction times for the linear spline $J(S)$ with $n=32$ and smoothing factor $\gamma=2\times10^{-18}$ that best fits a subset of the data reported in Fig. 4, with $SSD=0.86<\varepsilon=8.5$, (b) nucleation rates parameterized by linear splines that are consistent with experimental variations of 8.5.

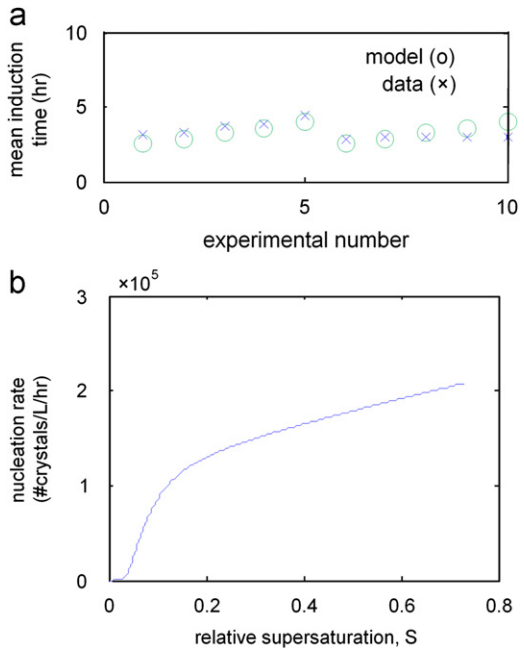

Fig. 8. (a) Best-fit mean induction times to the classical nucleation expression for a subset of the data reported in Fig. 4, with $A=475$, $B=0.04$, and $SSD=2.7<\varepsilon=8.5$, (b) the corresponding nucleation rate.

distribution of contaminants, so the distribution of the number of contminants per drop can be determined based on elementary statistical analysis (Pound and Lamer, 1952). Addressing the two-step nucleation mechanism is less straightforward — a truly first-principles approach model would include a model for the dynamic evolution of the liquid-liquid phase separation with the number and volume of droplets feeding into model (1). Having poorly mixed droplets would also be more involved, as then a first-principles approach would have to include a fluid mechanics model. In all of these cases, the overall approach proposed in the manuscript would remain the same but with (i) an extended mathematical model, (ii) multiple sets of bounds determined if multiple nucleation pathways are present, and (iii) more experimental data needed to be able to determine tight bounds on the nucleation rates.

4. Conclusions

The proposed approach for bounding of the nucleation rate enables the invalidation of proposed nucleation rate expressions while using only a small amount of compound and having the ability to collect data at high supersaturations such as occur in the dual-impinging-jet and vortex mixers used in the pharmaceutical industry for the manufacture of highly uniform crystals (Midler et al., 1994; Dauer et al., 1996; Mahajan and Kirwan, 1996; Lindrud et al., 2001; am Ende et al., 2003; Wang et al., 2006; Liu et al., 2008). The bounds constrain the nucleation rate expression, which can be fit to the experimental data and incorporated into simulation models for the design of crystallizers that employ process intensification (Schwarzer and Peukert, 2004; Liu et al., 2008; Woo et al., 2009). The numerical algorithm's use of a linear spline provides a high flexibility in capturing a wide variety of nucleation expressions, including the classical nucleation, power-law, and polynomial expressions. Applying the proposed approach to mean induction times for glycine in aqueous solution at high supersaturations indicated that the nucleation at high supersaturation was not consistent with a single classical nucleation mechanism occurring with uniform well-mixed droplets. An inability of any nucleation expression to fit the measured induction times for those experiments could be evidence for the lack of uniform concentration in each droplet or that contaminating particulates were located only a subset of droplets. Large gaps between the upper and lower bounds on the nucleation rate, as well as plots of the deviations between the best-fit models and measurements, indicate experimental conditions where additional experiments may be needed to improve the accuracy of the nucleation rate.

References

Aizenberg, J., Black, A.J., Whitesides, G.M., 1999. Control of crystal nucleation by patterned self-assembled monolayers. Nature 398, 495–498.
Allen, K., Davey, R.J., Ferrari, E., Towler, C., Tiddy, G.J., Jones, M.O., Pritchard, R.G., 2002. The crystallization of glycine polymorphs from emulsions, microemulsions, and lamellar phases. Cryst. Growth Des. 2, 523–527.
am Ende, D.J.; Crawford, T.C.; Weston, N.P. U.S. Patent 6,558,435, 2003.
Auer, S., Frenkel, D., 2001. Suppression of crystal nucleation in polydisperse colloids due to increase of the surface free energy. Nature 413 (6857), 711–713.
Baird, J.K., 1999. Theory of protein crystal nucleation and growth controlled by solvent evaporation. J. Cryst. Growth 204, 553–562.
Beck, J.V., Arnold, K.J., 1977. Parameter Estimation in Engineering and Science. John Wiley & Sons, New York.
Blow, D.M., Chayen, N.E., Lloyd, L.F., Saridakis, E., 1994. Control of nucleation of protein crystals. Protein Sci. 3, 1638–1643.
Cacciuto, A., Auer, S., Frenkel, D., 2004. Onset of heterogeneous crystal nucleation in colloidal suspensions. Nature 428, 404–406.
Chapra, S.C., Canale, R.P., 2002. Numerical Methods for Engineers, 4th Edn. McGraw-Hill, New York.
Chattopadhyay, S., Erdemir, D., Evans, J.M.B., Ilavsky, J., Amenitsch, H., Segre, C.U., Myerson, A.S., 2005. SAXS study of the nucleation of glycine crystals from a supersaturated solution. Cryst. Growth Des. 5, 523–527.
Chen, C., Cook, O., Nicholson, C.E., Cooper, S.J., 2011. Leapfrogging Ostwald's rule of stages: crystallization of stable gamma-glycine directly from microemullsions. Cryst. Growth Des. 11, 2228–2237.
Cinlar, E., 1971. Introduction to Stochastic Processes. Prentice-Hall: Englewood Cliffs, NJ.
Dauer, R.; Mokrauer, J.E.; McKeel, W. J. U.S. Patent 5,578,279, 1996.
Foster, W.R., Ungar, L.H., Schwaber, J.S., 1993. Significance of conductances in Hodgkin-Huxley models. J. Neurophysiol. 70, 2502–2518.
Goh, L.M. Dynamic analysis of pharmaceutical and biological systems from the nano- to microscale. M.S. Thesis, University of Illinois at Urbana-Champaign, Urbana, IL, USA, 2007.

Goh, L.M., Chen, K.J., Bhamidi, V., He, G., Kee, N.C.S., Kenis, P.J.A., Zukoski, C.F., Braatz, R.D., 2010. A stochastic model for nucleation kinetics determination in droplet-based microfluidic systems. Cryst. Growth Des. 10, 2515–2521.
Hansen, C.L., Classen, S., Berger, J.M., Quake, S.R., 2006. A microfluidic device for kinetic optimization of protein crystallization and in situ structure determination. J. Am. Chem. Soc. 128, 3142–3143.
He, G., Bhamidi, V., Wilson, S.R., Tan, R.B.H., Kenis, P.J.A., Zukoski, C.F., 2006. Direct growth of γ-glycine from neutral aqueous solutions by slow, evaporation-driven crystallization. Cryst. Growth Des. 6, 1746–1749.
Heath, M.T., 2002. Scientific Computing: An Introductory Survey, 2nd Edn. McGraw-Hill, New York.
Kelton, K.F., 1991. Crystal nucleation in liquids and glasses. In: Ehrenreich, H., Turnbull, D. (Eds.), Solid State Physics, Vol. 45. Academic Press, New York, pp. 75–178.
Kreutz, J.E., Li, L., Roach, L.S., Hatakeyama, T., Ismagilov, R.F., 2009. Laterally mobile, functionalized self-assembled monolayers at the fluorous-aqueous interface in a plug-based microfluidic system: characterization and testing with membrane protein crystallization. J. Am. Chem. Soc. 131, 6042–6043.
Laval, P., Giroux, C., Leng, J., Salmon, J.-B., 2008. Microfluidic screening of potassium nitrate polymorphism. J. Cryst. Growth 310, 3121–3124.
Li, L., Nachtergaele, S., Seddon, A.M., Tereshko, V., Ponomarenko, N., Ismagilov, R.F., 2008. Simple host-guest chemistry to modulate the process of concentration and crystallization of membrane proteins by detergent capture in a microfluidic device. J. Am. Chem. Soc. 130, 14324–14328.
Lindrud, M.D.; Kim, S.; Wei, C. U.S. Patent 6,302,958, 2001.
Liu, Y., Cheng, C.-Y., Liu, Y., Prud'homme, R.K., Fox, R.O., 2008. Mixing in a multi-inlet vortex mixer (MIVM) for flash nano-precipitation. Chem. Eng. Sci. 63, 2829–2842.
Mahajan, A.J., Kirwan, D.J., 1996. Micromixing effects in a two-impinging-jets precipitator. AIChE J. 42, 1801–1814.
Midler, M., Paul, E.L., Whittington, E.F., Futran, M., Liu, P.D., Hsu, J., Pan, S.-H. U.S. Patent 5,314,506, 1994.
Nielsen, A.E., 1964. Kinetics of Precipitation. Pergamon Press, Oxford.
Nyvlt, J., 1985. The Kinetics of Industrial Crystallization. Elsevier Science Pub. Co., Inc, Amsterdam.
Pound, G.M., Lamer, V.K., 1952. Kinetics of crystalline nucleus formation in supercooled liquid tin. J. Am. Chem. Soc. 74, 2323–2332.
Pusey, P.N., 1991. Colloidal suspensions. In: Hansen, J.P., Levesque, D., Zinn-Justin, J. (Eds.), Liquids, Freezing and the Glass Transition. Elsevier, New York, pp. 763–931. Chapter 10.
Saikumar, M.V., Glatz, C.E., Larson, M.A., 1998. Lysozyme crystal growth and nucleation kinetics. J. Cryst. Growth 187, 277–288.
Sanjoh, A., Tsukihara, T., 1999. Spatiotemporal protein crystal growth studies using microfluidic silicon devices. J. Cryst. Growth 196, 691–702.
Schope, H.J., Bryant, G., van Megen, W., 2006. Two-step crystallization kinetics in colloidal hard-sphere systems. Phys. Rev. Lett., 96. art no. 175701.
Schwarzer, H.C., Peukert, W., 2004. Combined experimental/numerical study on the precipitation of nanoparticles. AIChE J. 50, 3234–3247.
Squires, T.M., Quake, S.R., 2005. Microfluidics: fluid physics at the nanoliter scale. Rev. Mod. Phys. 77, 977–1026.
Talreja, S., Kim, D.Y., Mirarefi, A.Y., Zukoski, C.F., Kenis, P.J.A., 2005. Screening and optimization of protein crystallization conditions through gradual evaporation using a novel crystallization platform. J. Appl. Crystallogr. 38, 988–995.
Talreja, S., Kenis, P.J.A., Zukoski, C.F., 2007. A kinetic model to simulate protein crystal growth in an evaporation-based crystallization platform. Langmuir 23, 4516–4522.
Taylor, J.R., 1982. Introduction to Error Analysis: The Study of Uncertainties in Physical Measurements. University Science Books, Sausalito, CA.
ten Wolde, P.R., Frenkel, D., 1997. Enhancement of protein crystal nucleation by critical density fluctuations. Science 277, 1975–1978.
Teychené, S., Biscans, B., 2011. Microfluidic device for the crystallization of organic molecules in organic solvents. Cryst. Growth Des. 11, 4810–4818.
Vekilov, P.G., 2004. Dense liquid precursor for the nucleation of ordered solid phases from solution. Cryst. Growth Des. 4, 671–685.
Vekilov, P.G., 2010. Nucleation. Cryst. Growth Des. 10, 5007–5019.
Vekilov, P.G., Galkin, O., 2003. On the methods of determination of homogeneous nucleation rates of protein crystals. Colloids Surf. A 215, 125–130.
Volmer, M., Weber, A., 1926. Keimbildung in übersättigten Gebilden. Z. Phys. Chem. 119, 277–301.
Walton, A.G., 1969. Nucleation in Liquids and Solutions. In: Zettlemoyer, A.C. (Ed.), Nucleation. Marcel Dekker, New York, pp. 238.
Wang, X., Gillian, J.M., Kirwan, D.J., 2006. Quasi-emulsion precipitation of pharmaceuticals. 1. Conditions for formation and crystal nucleation and growth behavior. Cryst. Growth Des. 6, 2214–2227.
Woo, X.Y., Tan, R.B.H., Braatz, R.D., 2009. Modeling and computational fluid dynamics-population balance equation-micromixing simulation of impinging jet crystallizers. Cryst. Growth Des. 9, 156–164.
Zheng, B., Roach, L.S., Ismagilov, R.F., 2003. Screening of protein crystallization conditions on a microfluidic chip using nanoliter-size droplets. J. Am. Chem. Soc. 125, 11170–11171.